Supplementary Information (SI) for ChemComm.
This journal is © The Royal Society of Chemistry 2026

Supporting Information

Experimental section

Synthesis of Co(II)meso-tetra(4-cyanobenzyl)porphine

In a 1000 mL three-neck round-bottom flask, 4-cyanobenzaldehyde (26.2260 g, 200 mmol) was dissolved in propionic acid (600 mL). The mixture was stirred under an N_2 atmosphere and heated to reflux in an oil bath at 150 ℃. Freshly distilled pyrrole (200 mmol) was then added dropwise, and the reaction mixture was maintained under these conditions for 1.0 h. Afterward, the mixture was stirred and cooled to room temperature. Methanol (300 mL) was added, and stirring was continued for an additional 1 h. The resulting suspension was allowed to stand for 24 h. The precipitate was collected by vacuum filtration and washed with methanol (5 × 150 mL) until the filtrate became colorless and clear, affording a purple solid. The crude product was further purified by silica gel column chromatography, concentrated under reduced pressure, and dried under vacuum to give a purple solid.

In a 250 mL three-neck round-bottom flask, 5,10,15,20-tetrakis(4-cyanophenyl)porphyrin (T(4-CN)PP) (0.2859 g, 0.40 mmol) and anhydrous cobalt acetate (0.7081 g, 4.0 mmol) were dissolved in DMF (120 mL). The reaction mixture was stirred under an N_2 atmosphere and heated to 140 ℃ for 24.0 h. After natural cooling to room temperature, the resulting mixture was collected by vacuum filtration. The obtained solid was dissolved in dichloromethane (100 mL), and the resulting solution was washed with distilled water (4 × 100 mL) until the upper aqueous phase became clear. The separated organic layer was dried over anhydrous Na_2SO_4 and concentrated under reduced pressure. The product was purified by silica gel column chromatography and dried in a vacuum oven at 80 ℃ for 8.0 h to afford a red powder (Co(II)meso-tetra(4-cyanobenzyl)porphine).

Synthesis of $Bi_{19}S_{27}Br_3$ nanorods.

In a typical procedure, $Bi(NO_3)_3{\cdot}5H_2O$ (0.15 mmol), thiourea (5 mmol), and $[C_{16}mim]Br$ (1.549 g) were dissolved in ethylene glycol (40 mL) and stirred vigorously at room temperature for 1 h in air. Then the mixed solution was transferred into a 50

mL Teflon-lined stainless-steel autoclave, sealed, and heated at 130 °C for 12 h. After natural cooling to room temperature, the obtained precipitate was collected by centrifugation, washed thoroughly with deionized water and ethanol to remove residual ions, and dried at 60 °C for 12 h prior to further characterization.

Synthesis of TCBP(Co)/$Bi_{19}S_{27}Br_3$ composites

The synthesis of TCBP(Co) was carried out as described in the Supporting Information. The TCBP(Co)/$Bi_{19}S_{27}Br_3$ composites were prepared via an oil-bath-assisted assembly method, as illustrated in Fig. 1a. Briefly, 0.1 g $Bi_{19}S_{27}Br_3$ powder was stirred in 20 mL of ethanol and stirred for 20 min. Subsequently, a designated volume (100, 200, 400, or 600 μL) of TCBP(Co) ethanol solution (0.5 $g \cdot L^{-1}$) was added dropwise to the above suspension under continuous stirring for 10 min. The resulting mixture was then transferred to an oil bath and maintained at 60 °C for 6 h to facilitate composite formation. After the reaction, the product was cooled to room temperature, collected by centrifugation, washed thoroughly with ethanol, and dried at 60 °C to yield the final TCBP(Co)/$Bi_{19}S_{27}Br_3$ composites.

The obtained samples were labeled as TCBP(Co)/$Bi_{19}S_{27}Br_3$-1, TCBP(Co)/$Bi_{19}S_{27}Br_3$-2, TCBP(Co)/$Bi_{19}S_{27}Br_3$-3 and TCBP(Co)/$Bi_{19}S_{27}Br_3$-4, corresponding to TCBP(Co) solution volumes of 100, 200, 400, and 600 μL, respectively.

Characterizations

X-ray diffraction (XRD) patterns were recorded on a Shimadzu XRD-6000 diffractometer using Cu Kα radiation. The scanning electron microscopy (SEM) was taken on JSM-7800F and ThermoFisher Apreo SHiVac. The Transmission electron microscopy (TEM) images were characterized by JEOL-JEM-2100. The high-resolution TEM (HR-TEM) micrographs were obtained by FEI Tecnai G2 F20 S-TWIN Electron Microscope. The UV-vis diffuse reflectance spectra (DRS) were recorded using a Shimadzu UV-2450 spectrometer. The Fourier transform infrared (FT-IR) spectra were conducted on Nexus 470 FT-IR spectrometer. The X-ray photoelectron spectroscopy (XPS) was investigated by PHI5300 instrument with a Mg Kα source. The in-situ FT-IR spectra were acquired with a ThermoFisher Nicolet iZ10. The

Electrochemical studies were conducted by electrochemical workstation (CHI760E) with a three-electrode configuration. Conductive glass coated with the catalyst dispersion was used as the working electrode. The Pt rod acted as a counter electrode, and Ag/AgCl electrode with saturated KCl solution was used as a reference electrode. The photocurrent responses curves were measured in 0.1 mol/L phosphate buffer solution (pH = 7), using a 300 W Xenon lamp as the light source during test. The electrochemical impedance spectra (EIS) were performed in a prepared electrochemical impedance solution (0.1 mol/L KCl solution, containing 5 mmol containing 5 mmol L^{-1} $[Fe(CN)_6]^{3-}$/$[Fe(CN)_6]^{4-}$. The Mott-Schottky plots were obtained in 0.2 mol/L Na2SO4 solution with an amplitude of 5 mV, the test frequency was kept at 2000, 2500, and 3000 Hz successively.

Photocatalytic measurement of CO_2 reduction

In the photocatalytic conversion of CO_2, the experiments were performed at the Labsolar-6A system (Perfect Light Co., China). The sample (10 mg) was uniformly applied to a 47 mm diameter disc of high-purity quartz fiber, which was placed on a quartz tripod and placed in a quartz glass reactor. Air was removed by several vacuum treatments and feeding of high-purity CO_2. After a dark reaction for 30 min, the photocatalytic reaction was measured under the irradiation of a 300 W Xe lamp with a constant temperature water bath at 10 °C. The gas products were detected by gas chromatography (Changzhou Pana Instrument Co., Ltd.).

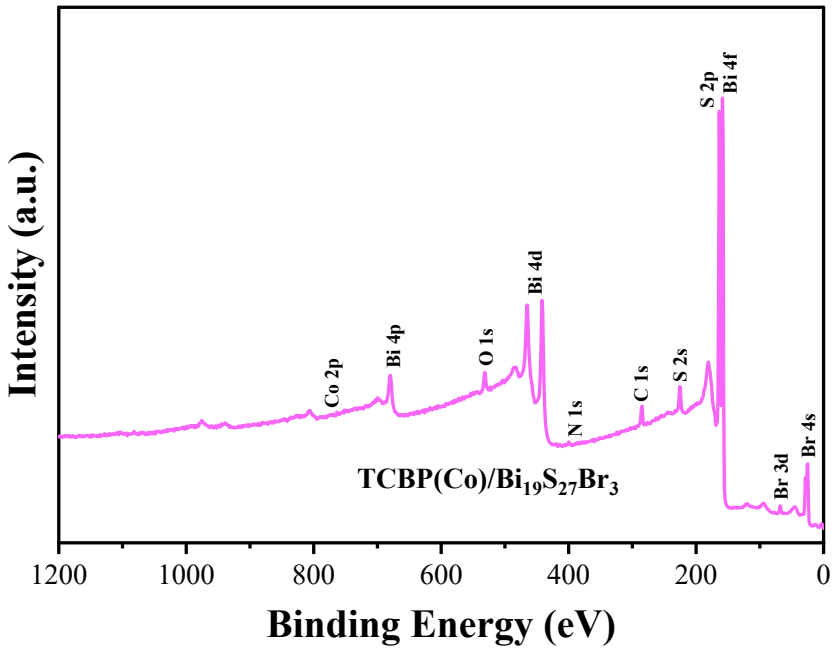

Fig. S1 XPS full spectrum of the TCBP(Co)/$Bi_{19}S_{27}Br_3$-3.

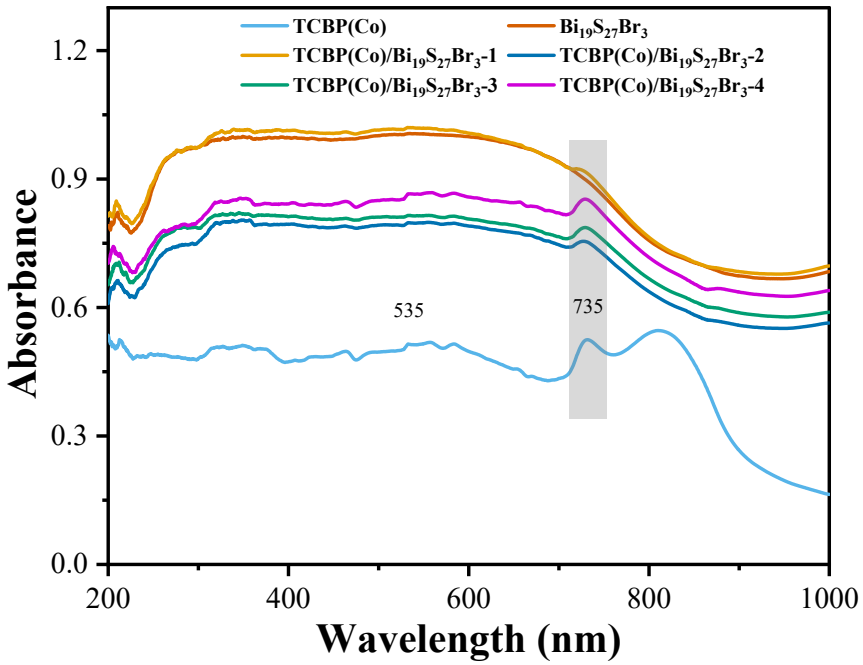

Fig. S2 UV-vis diffuse reflectance spectra of $Bi_{19}S_{27}Br_3$, TCBP(Co) and TCBP(Co)/$Bi_{19}S_{27}Br_3$-x (x = 1–4).

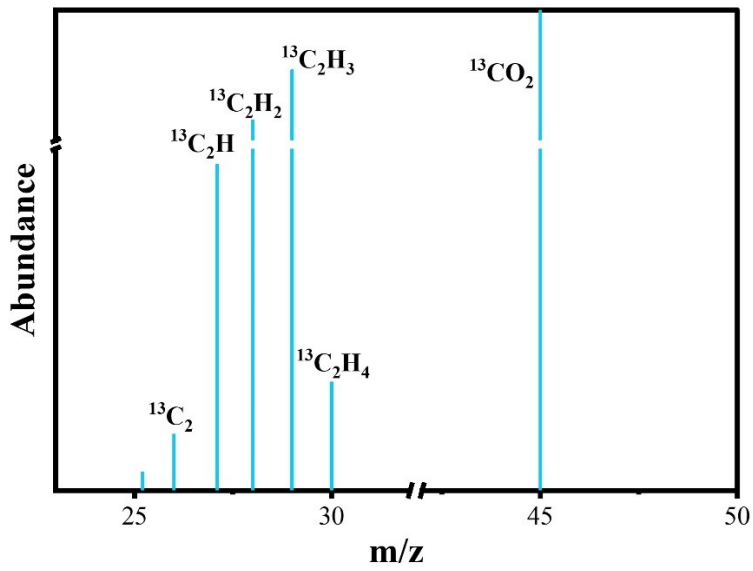

Fig. S3 GC–MS spectra of C_2H_4 from photocatalytic reduction of $^{13}CO_2$

To directly address this issue, we have performed a $^{13}CO_2$ isotope labeling experiment. The gas products were analyzed by GC-MS. As shown in Fig. S3, under $^{13}CO_2$ atmosphere, a distinct molecular ion peak assigned to $^{13}C_2H_4$ appears at m/z = 30, accompanied by a series of characteristic fragment signals at m/z = 29, 28, 27 and 26, corresponding to $^{13}C_2H_3$, $^{13}C_2H_2$, $^{13}C_2H$ and $^{13}C_2$, respectively.[1, 2] Meanwhile, the strong signal at m/z = 45 is attributed to $^{13}CO_2$, confirming that the photocatalytic reaction takes place in an environment containing isotopically labelled CO_2. The detection of ^{13}C labeled C_2H_4 and its fragments gave direct evidence for the origin of the product. It confirmed that C_2H_4 was formed from CO_2 reduction, rather than from carbon residues or organic contaminants.

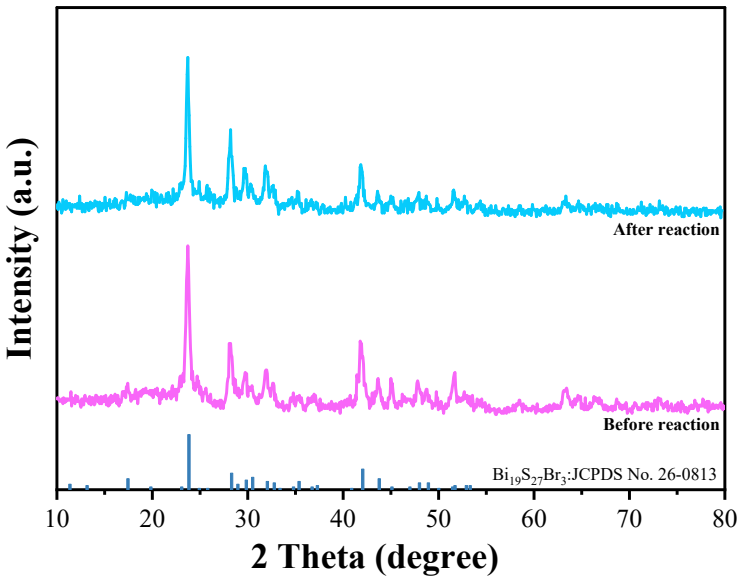

Fig. S4 XRD patterns of TCBP(Co)/$Bi_{19}S_{27}Br_3$-3 before and after the stability test.

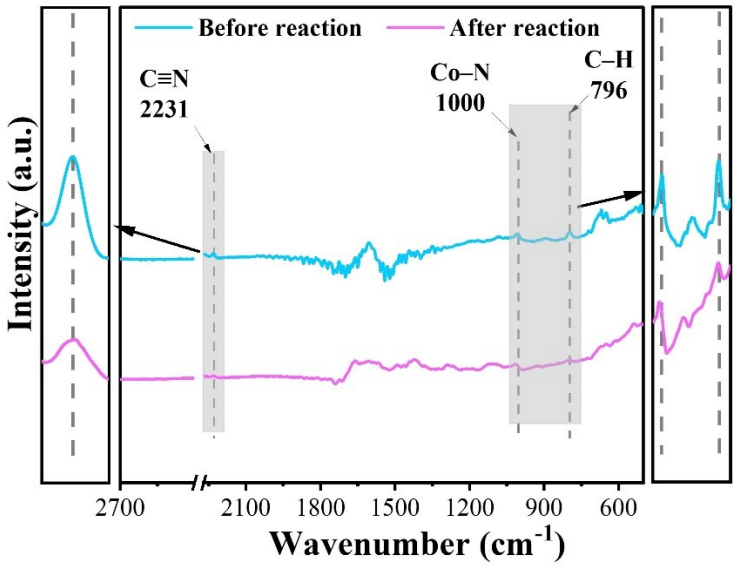

Fig. S5 FTIR spectra of TCBP(Co)/$Bi_{19}S_{27}Br_3$-3 before and after the stability test.

The structural durability of TCBP(Co)/$Bi_{19}S_{27}Br_3$-3 was further evaluated by FTIR spectroscopy after the photocatalytic stability test. As shown in Fig. S5, the characteristic vibrations of the TCBP(Co) component are well preserved after reaction, including the C≡N stretching band at 2231 cm^{-1}, the Co–N coordination related vibration around 1000 cm^{-1}, and the aromatic C–H vibration at 796 cm^{-1}. This result indicates that the molecular framework and Co–N coordination environment of TCBP(Co) are largely maintained during the photocatalytic CO_2 reduction process.

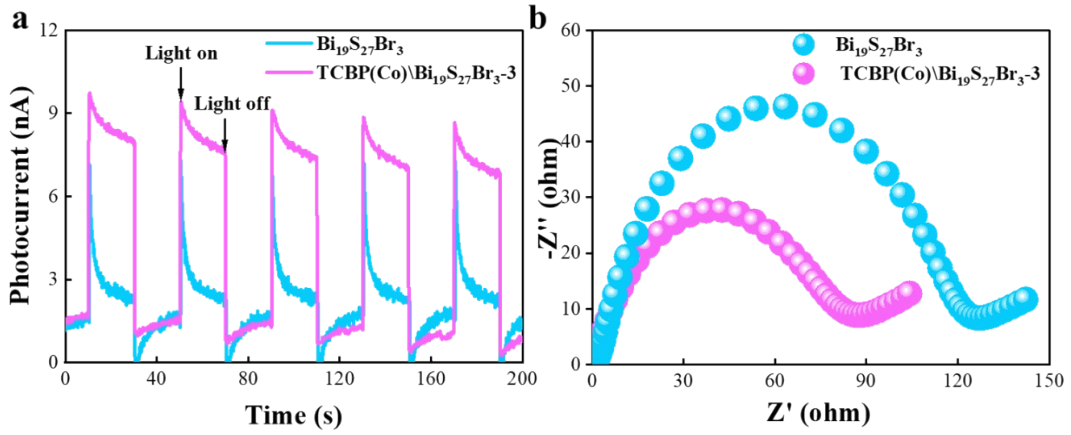

Fig. S6 (a) Transient photocurrent response spectra; (b) EIS spectra of $Bi_{19}S_{27}Br_3$ and TCBP(Co)/$Bi_{19}S_{27}Br_3$-3.

TCBP(Co)/$Bi_{19}S_{27}Br_3$-3 exhibits the highest photocurrent response value (Fig. S6a), demonstrating that more free electrons are generated and transferred to participate in the surface reaction. TCBP(Co)/$Bi_{19}S_{27}Br_3$-3 exhibits the smallest Nyquist arc radius, implying the lowest interfacial charge trans fer resistance (Fig. S6b).

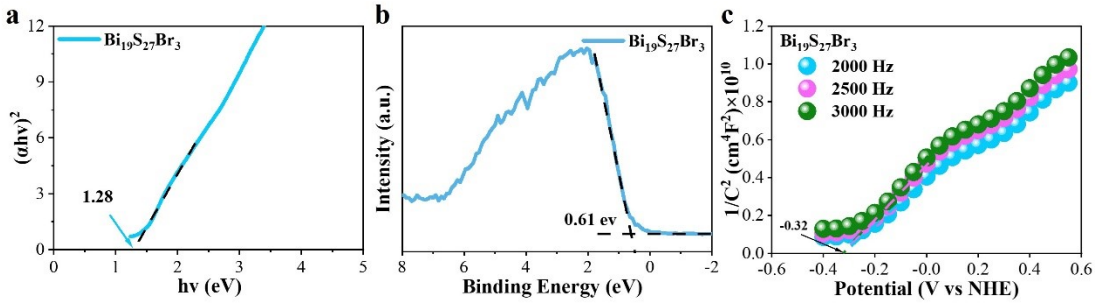

Fig. S7 (a) Tauc plots; (b) XPS valence band spectra of prepared materials; (c) Mott–Schottky plots of $Bi_{19}S_{27}Br_3$.

The band gap (E_g) of the $Bi_{19}S_{27}Br_3$ materials was calculated to be 1.28 eV based on the Tauc plot derived from the UV-Vis diffuse reflectance spectrum data(Fig. S7a). To further elucidate the electronic band structure, Mott–Schottky (M–S) analysis was performed (Fig. S7c). The M–S plot of $Bi_{19}S_{27}Br_3$ exhibited a positive slope, characteristic of an n type semiconductor, and its flat band potential was determined to be –0.32 V vs. NHE (pH = 7). Since the flat band potential of an n type semiconductor approximates its Fermi level, this value was used as the Fermi level of $Bi_{19}S_{27}Br_3$.[3]

Additionally, the valence band (E_{VB}) position of $Bi_{19}S_{27}Br_3$ was determined via XPS. As shown in Fig. S7b, the valence band maximum lies 0.61 eV below the Fermi level. Combining this with the M–S result, the E_{VB} position is calculated to be 0.29 V vs. NHE. Based on the bandgap value of 1.28 eV, the conduction band (E_{CB}) is then derived using the relation $E_{CB} = E_{VB} - E_g$, yielding an E_{CB} of –0.99 V vs. NHE.[4] These findings confirm the favorable band alignment and narrow bandgap of $Bi_{19}S_{27}Br_3$, which, when integrated with TCBP(Co), can enhance visible light absorption and facilitate efficient charge separation, thereby promoting photocatalytic activity.

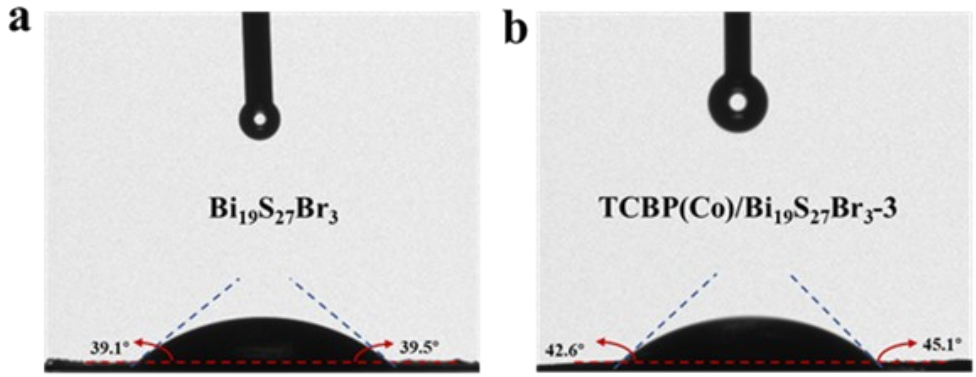

Fig. S8 Water contact angle images of the prepared materials, (a) $Bi_{19}S_{27}Br_3$; (b) TCBP(Co)/$Bi_{19}S_{27}Br_3$-3

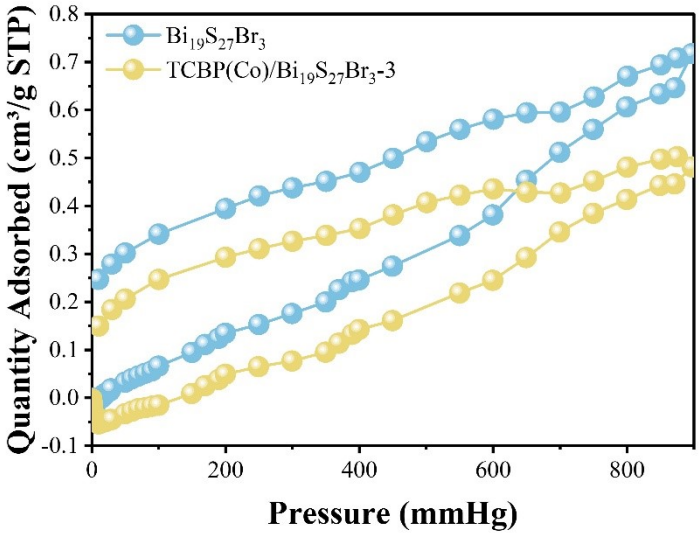

Fig. S9 CO_2 adsorption–desorption isotherms of $Bi_{19}S_{27}Br_3$ and TCBP(Co)/$Bi_{19}S_{27}Br_3$-3.

The pristine $Bi_{19}S_{27}Br_3$ exhibits a higher equilibrium CO_2 adsorption capacity than TCBP(Co)/$Bi_{19}S_{27}Br_3$-3, indicating that the introduction of TCBP(Co) does not simply enhance the total physical uptake of CO_2. This decrease may be related to partial surface coverage or occupation of accessible adsorption sites by the porphyrin molecules. However, the photocatalytic CO_2 reduction performance is not solely determined by the total CO_2 adsorption capacity, but also strongly depends on the activation of adsorbed CO_2 molecules and the efficiency of interfacial charge transfer. [5] Although TCBP(Co)/$Bi_{19}S_{27}Br_3$ shows a lower total CO_2 uptake, the Co–N_4 sites and the improved interfacial electronic interaction may facilitate the conversion of adsorbed CO_2 into reactive intermediates.

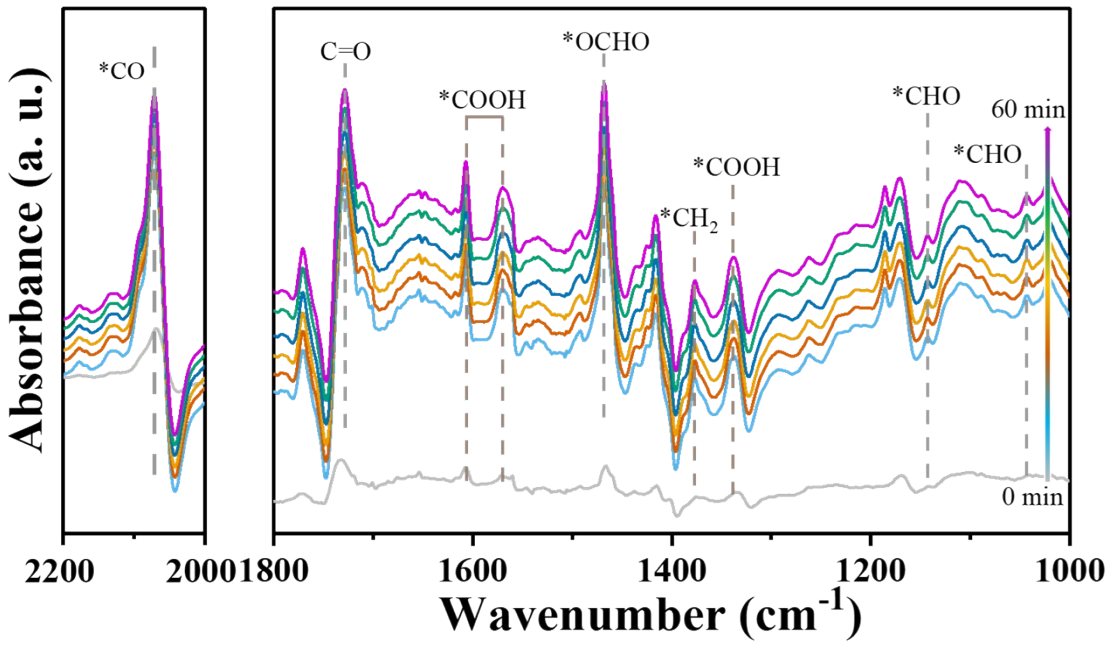

Fig. S10 *In situ* FTIR spectra of $Bi_{19}S_{27}Br_3$.

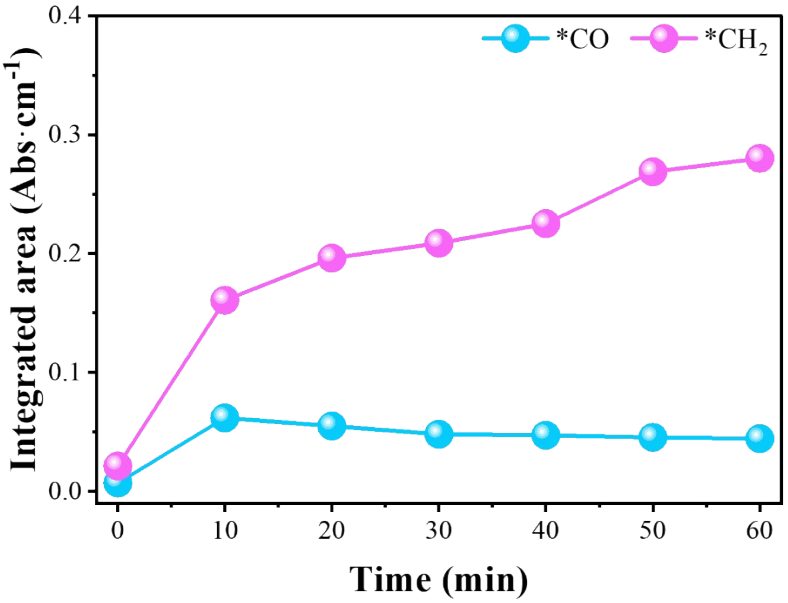

Fig. S11 Peak area evolution of the *CO and *CH_2 signals from *in situ* FTIR spectra.

Table S1 Comparison of CO_2 photoreduction performance of reported materials

Photocatalysts	Used amount (mg)	Light source	Reduction mode	Reduction medium	Products (μmol g^{-1} h^{-1})	Ref
TiO_2/SBA-15@Co-TCPP	20	300 W Xe lamp	Liquid-solid	acetonitrile solution and triethanolamine	CO: ~241.63 H_2: ~176	6
$CsPbBr_3$⊆Pb-TCPP	10	300 W Xe lamp	Liquid-solid	Acetonitrile, benzylamine and deionized water	CO: ~ 67.50 CH_4: ~ 13.28	7
CoTPPS/$ZnIn_2S_4$	5	LED light	Liquid-solid	anhydrous acetonitrile and water	CO: ~ 388.26	8
CuTCPP/TiO_2	5	300 W Xe lamp	Liquid-solid	water	CO: ~ 73	9
1-TA/C-ZCF	10	300 W Xe lamp	Liquid-solid	triethanolamine and water	CO: ~ 392.23 CH_4: ~ 34.55	10
Co-TCPP/Bi_3O_4Br	20	300 W Xe lamp	Liquid-solid	water	CO: ~ 71.3	11
NiTMCPP/BiOBr	30	300 W Xe lamp	Liquid-solid	water	CO: ~2.83 CH_4: ~0.02	12
F-TotPp(Co)	30	300 W Xe lamp	Liquid-solid	water	CO: ~ 0.52 C_2H_4: ~ 0.06	13
PFC-11(Cu)	30	300 W Xe lamp	Liquid-solid	water	CO: ~ 0.12 CH_4: ~ 0.24	14
$Bi_{19}S_{27}Br_3$@$SnIn_4S_8$	50	300 W Xe lamp	Gas-solid	water	CO: ~35.63	15
$Bi_{19}S_{27}Br_3$/g-C_3N_4	30	300 W Xe lamp	Liquid-solid	water	CO: ~12.87	16
$Bi_{19}S_{27}Br_3$/CoAl-LDH	50	300 W Xe lamp	Liquid-solid	water	CO: ~ 86.41 CH_4: ~ 1.09	17
TCBP(Co)/$Bi_{19}S_{27}Br_3$-3	10	300 W Xe lamp	Gas-solid	water	CO: ~0.42 C_2H_4: ~2.7	**This work**

References

1. Y. Wu, Q. Chen, J. Zhu, K. Zheng, M. Wu, M. Fan, W. Yan, J. Hu, J. Zhu, Y. Pan, X. Jiao, Y. Sun and Y. Xie, *Angew. Chem. Int. Ed.*, 2023, **62**, e202301075.
2. H. Du, Y. Fu, R. Shi, Z. Cao, S. Zhang, K. Liu, J. Wang, B. Jiang and H. Li, *Angew. Chem. Int. Ed.*, 2026, **65**, e20354.
3. G. Liu, L. Li, B. Wang, N. Shan, J. Dong, M. Ji, W. Zhu, P. K. Chu, J. Xia and H. Li, *Acta Phys. Chim. Sin.*, 2024, **40**, 2306041.
4. G. Liu, L. Li, B. Wang, J. Yang, J. Dong, N. Shan, W. Zhu, J. Xia and H. Li, *Appl. Surf. Sci.*, 2024, **660**, 159924.
5. Y. Liu, R. Zou, Z. Chen, W. Tu, R. Xia, E. I. Iwuoha and X. Peng, *ACS Catal.*, 2024, **14**, 138-147.
6. M.-Y. Nan, H. Rao, P. She and J.-S. Qin, *Chem. Eng. J.*, 2024, **500**, 157419.
7. Y.-G. Luo, C.-L. Peng, L.-B. Tang, J.-Y. Zhang, H.-Z. Wang, Y.-F. Liu, Q.-F. Ke, Y.-Z. Fang and N. Zhang, *Chem. Eng. J.*, 2024, **495**, 153307.
8. Y. Qi, S. Li, T. Bao, P. She, H. Rao and J.-s. Qin, *Appl. Catal. B Environ. Energy*, 2024, **357**, 124299.
9. F. Yue, M. Shi, C. Li, Y. Meng, S. Zhang, L. Wang, Y. Song, J. Li and H. Zhang, *J. Colloid Interface Sci.*, 2024, **665**, 1079-1090.
10. M. Wang, Y. Zhang, D. Chen, N. Li, Q. Xu, H. Li and J. Lu, *Chem. Eng. J.*, 2023, **469**, 144064.
11. Y. Zhang, F. Guo, K. Wang, J. Di, B. Min, H. Zhu, H. Chen, Y.-X. Weng, J. Dai, Y. She, J. Xia and H. Li, *Chem. Eng. J.*, 2023, **465**, 142663.
12. L. Li, G. Liu, S. Cao, J. Dong, B. Wang, Y. She, J. Xia and H. Li, *Appl. Catal. B Environ. Energy*, 2025, **365**, 124904.
13. K. Wang, Q. Li, X. Chen, Z. Li, Y.-F. Yang, T.-S. Zhang, H.-M. Shen, Q. Wang, B. Wang, Y. Zhang, J. Xia, H. Li and Y. She, *Appl. Catal. B Environ. Energy*, 2025, **362**, 124765.
14. M. Zhou, D. Ding, Y. Shi, K. Wang, Q. Wang, X. Chen, H.-M. Shen, T.-S. Zhang, Y.-F. Yang, J. Xia, H. Li and Y. She, *Chem. Eng. J.*, 2025, **503**, 158501.
15. W. Jia, R. Xiong, Y. Sun, Y. Xiao, B. Cheng and S. Lei, *J. Mater. Chem. A*, 2024, **12**, 4513-4524.
16. J. Zhao, M. Ji, H. Chen, Y.-X. Weng, J. Zhong, Y. Li, S. Wang, Z. Chen, J. Xia and H. Li, *Appl. Catal. B Environ. Energy*, 2022, **307**, 121162.
17. J. Hua, C. Ma, D. Wu, H. Huang, X. Dai, K. Wu, H. Wang, Z. Bian and S. Feng, *J. Alloys Compd.*, 2024, **970**, 172516.